

Fermi National Accelerator Laboratory

FERMILAB-Pub-99/269-E

E815

Evidence for Diffractive Charm Production in ν_μ Fe and $\bar{\nu}_\mu$ Fe Scattering at the Tevatron

T. Adams et al.
The E815 Collaboration

*Fermi National Accelerator Laboratory
P.O. Box 500, Batavia, Illinois 60510*

October 1999

Submitted to *Physical Review D*

Disclaimer

This report was prepared as an account of work sponsored by an agency of the United States Government. Neither the United States Government nor any agency thereof, nor any of their employees, makes any warranty, expressed or implied, or assumes any legal liability or responsibility for the accuracy, completeness, or usefulness of any information, apparatus, product, or process disclosed, or represents that its use would not infringe privately owned rights. Reference herein to any specific commercial product, process, or service by trade name, trademark, manufacturer, or otherwise, does not necessarily constitute or imply its endorsement, recommendation, or favoring by the United States Government or any agency thereof. The views and opinions of authors expressed herein do not necessarily state or reflect those of the United States Government or any agency thereof.

Distribution

Approved for public release; further dissemination unlimited.

Copyright Notification

This manuscript has been authored by Universities Research Association, Inc. under contract No. DE-AC02-76CH03000 with the U.S. Department of Energy. The United States Government and the publisher, by accepting the article for publication, acknowledges that the United States Government retains a nonexclusive, paid-up, irrevocable, worldwide license to publish or reproduce the published form of this manuscript, or allow others to do so, for United States Government Purposes.

Evidence for Diffractive Charm Production in $\nu_\mu Fe$ and $\bar{\nu}_\mu Fe$ Scattering at the Tevatron

T. Adams, A. Alton, T. Bolton, J. Goldman, M. Goncharov, D. Naples*
Kansas State University, Manhattan, KS, 66506

R. A. Johnson, M. Vakili,† V. Wu
University of Cincinnati, Cincinnati, OH, 45221

J. Conrad, J. Formaggio, S. Koutsoliotas,‡ J. H. Kim,§ C. McNulty, A. Romosan,** M. H. Shaevitz,
P. Spentzouris,†† E. G. Stern, B. Tamminga, A. Vaitaitis, E. D. Zimmerman
Columbia University, New York, NY, 10027

R. H. Bernstein, L. Bugel, M. J. Lamm, W. Marsh, P. Nienaber,‡‡ J. Yu
Fermi National Accelerator Laboratory, Batavia, IL, 60510

L. de Barbaro, D. Buchholz, H. Schellman, G. P. Zeller
Northwestern University, Evanston, IL, 60208

J. Brau, R. B. Drucker, R. Frey, D. Mason
University of Oregon, Eugene, OR, 97403

S. Avvakumov, P. de Barbaro, A. Bodek, H. Budd, D. A. Harris,†† K. S. McFarland, W. K. Sakumoto, U. K. Yang
University of Rochester, Rochester, NY, 14627
(October 4, 1999)

We present evidence for the diffractive processes $\nu_\mu Fe \rightarrow \mu^- D_S^+ (D_S^0) Fe$ and $\bar{\nu}_\mu Fe \rightarrow \mu^+ D_S^- (D_S^0) Fe$ using the Fermilab SSQT neutrino beam and the Lab E neutrino detector. We observe the neutrino trident reactions $\nu_\mu Fe \rightarrow \nu_\mu \mu^- \mu^+ Fe$ and $\bar{\nu}_\mu Fe \rightarrow \bar{\nu}_\mu \mu^+ \mu^- Fe$ at rates consistent with Standard Model expectations. We see no evidence for neutral-current production of J/ψ via either diffractive or deep inelastic scattering mechanisms.

PACS 13.15+g, 12.15.-y, 13.60.Le, 12.40.Vv

(Submitted to Physical Review D)

I. INTRODUCTION

Opposite-signed two-muon production in deep inelastic scattering (DIS) with neutrinos or anti-neutrinos serves as a reliable signal for charm quark production through the sequence

$$\nu_\mu N \rightarrow \mu^- DX, \quad D \rightarrow \mu^+ \nu_\mu X', \quad (1.1)$$

where D represents a stable charmed hadron. This is

especially true in dense targets such as the NuTeV detector at Fermilab where absorption of pions and kaons in the hadronic shower suppresses backgrounds from meson decay that occur via

$$\nu_\mu N \rightarrow \mu^- \pi^+ (K^+) X; \quad \pi^+ (K^+) \rightarrow \mu^+ \nu_\mu. \quad (1.2)$$

Previous studies of DIS two-muon production in neutrino interactions have yielded important measurements of the CKM matrix elements V_{cd} and V_{cs} , the effective charm quark mass, and the size and shape of the nucleon strange sea. These studies were performed in the context

*Present Address: University of Pittsburgh, Pittsburgh, PA, 15260

†Present Address: Texas A&M University, College Station, TX, 77843

‡Present Address: Bucknell University, Lewisburg, PA, 17837

§Present Address: University of California, Irvine, CA, 92697

**Present Address: University of California, Berkeley, CA, 94720

††Present Address: Fermi National Laboratory, Batavia, IL, 60510

‡‡Present Address: Marquette University, Milwaukee, WI, 53201

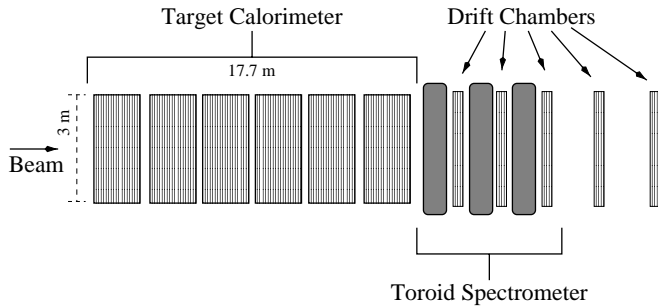


FIG. 1. Schematic drawing of the Lab E detector. Beam enters from the left. The target/calorimeter is on the left and the toroid spectrometer is on the right.

of the QCD-corrected quark-parton model and hence were restricted to large values of energy transfer, ν , to the struck nucleon resulting in large amounts of observed hadronic energy, E_{HAD} .

At low hadronic energy, one expects to observe charm production via another mechanism, namely, diffractive production of pseudoscalar and vector D_S mesons via both coherent and incoherent scattering:

$$\nu_\mu A \rightarrow \mu^- D_S^+ A, \quad \nu_\mu A \rightarrow \mu^- D_S^+ \gamma_{\text{SOFT}} A, \quad (1.3)$$

where the low energy decay photon γ_{SOFT} will accompany production of vector D_S^* , $A = Fe$ for coherent production in our experiment, and $A = n$ or p for incoherent production. Here, large energy transfer to the meson may not result in large hadronic energy because the nucleus remains intact.

These reactions have been observed at the few event level in bubble chamber and emulsion experiments [1,2]. It is important to understand the size of this diffractive contribution because of its influence as a background to DIS charm production. These processes are also of interest to future high statistics neutrino experiments at a muon collider. They provide the possibility of measuring the ratio V_{cd}/V_{cs} via comparison of the rates $\nu_\mu A \rightarrow \mu^- D^{*+} A$ and $\nu_\mu A \rightarrow \mu^- D_S^{*+} A$. Additionally, they can create a signature which mimics quasi-elastic production of τ -leptons through the chain $\nu_\mu A \rightarrow \mu^- D_S^+ (\gamma_{\text{SOFT}}) A$, $D_S^+ \rightarrow \tau^+ \nu_\tau$, which may be of concern to high sensitivity $\nu_\mu \rightarrow \nu_\tau$ oscillation searches.

A competing reaction that produces the same experimental signature, an opposite-signed muon pair with vanishing E_{HAD} , is the neutrino trident process [3,4]:

$$\nu_\mu A \rightarrow \mu^- \mu^+ \nu_\mu A. \quad (1.4)$$

In principle, the neutrino trident reaction provides an interesting test of electroweak theory since contributions from W and Z decay produce a reliably calculable 40% destructive interference effect. In practice, the very small cross-section implies that only a handful of neutrino tridents have previously been observed in neutrino scattering. Furthermore, the neutrino trident process must be considered in combination with the expected signal from

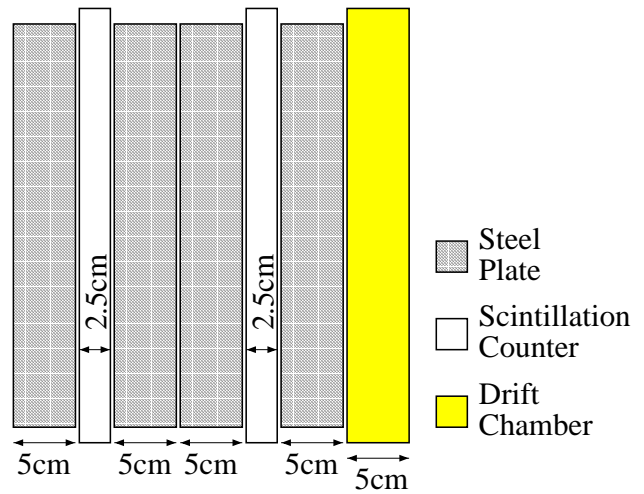


FIG. 2. Drawing of one segment of the Lab E calorimeter.

diffractive charm production in experiments that are only sensitive to two-muon final states. This point has not been recognized in previous measurements of neutrino tridents.

NuTeV (Fermilab Experiment E815) is a high-statistics experiment studying neutrino and anti-neutrino interactions with a high intensity, high energy sign-selected beam. Its primary goal is to measure the electroweak mixing angle $\sin^2 \theta_W$; however, the high-statistics nature makes it possible to study the rarer processes described above. At low (zero) hadronic energy the dominant deep-inelastic scattering (DIS) processes fall off and additional channels such as diffractive $D_S^\pm/D_S^{*\pm}$ production [2], neutrino trident [3,4], and diffractive J/ψ [5] become more important. This is the first analysis to study the inclusive production of all processes in the final state with low hadronic energy and two muons.

The next section will describe the NuTeV experiment while Section III details the data selection. Predictions for the sources of low- E_{HAD} two muons events are given in Section IV. Section V details the charged- and neutral-current analyses and conclusions are stated in the final section.

II. THE NUTEV EXPERIMENT

The NuTeV experiment ran at Fermilab using the refurbished Lab E detector [6] and ν_μ and $\bar{\nu}_\mu$ beams provided by the newly installed Sign-Selected Quadrupole Train (SSQT) [7]. The SSQT has the capability of selecting either muon neutrino or muon anti-neutrino beams while leaving $\lesssim 2 \times 10^{-3}$ of the anti-selected type.

The Lab E detector, located 1.5 km downstream of the primary target, consists of a target/calorimeter followed by a toroid spectrometer (Fig. 1). The calorimeter is composed of 42 segments of four steel plates, two liquid scintillator counters (SC) and one drift chamber (DC) (Fig. 2). The steel provides mass for the neutrino target,

the SC measure the longitudinal vertex and energy deposition (E), and the DC are used to find the transverse vertex

and reconstruct downstream tracks. Because of the high density of the target, only muons deeply penetrate the calorimeter, and all other particles create a hadronic or electromagnetic shower near the interaction vertex.

The toroid spectrometer, located immediately downstream of the calorimeter, focuses muons from the primary charged-current vertex given the type of beam (ν_μ or $\bar{\nu}_\mu$), measuring both charge and momentum (p) of muons with $p \geq 5$ GeV/c which enter the spectrometer. It is also possible to measure the momentum of a subset of muons with $5 \leq p \leq 15$ GeV/c which range out in the calorimeter, and to place a lower bound on the momentum of muons which exit the side of the calorimeter.

The NuTeV detector was calibrated with a separate beam of hadrons, muons, or electrons throughout the running period of the experiment. Hadronic and muon energy scales for the calorimeter were determined to 0.43% and 1.0% respectively over the energy range 5–200 GeV [8]. Muon momentum measurement in the spectrometer is limited by multiple Coulomb scattering to $\Delta p/p = 0.11$, and the sampling-dominated hadronic resolution was approximately $\Delta E/E = 0.86/\sqrt{E}$.

III. EVENT SELECTION

Analyses presented here use the full NuTeV data sample from the 1996-1997 fixed-target run corresponding to 1.3×10^{18} protons on target (POT) for neutrino running and 1.6×10^{18} protons on target for anti-neutrino running. The size of various event samples from NuTeV are listed in Table I.

Events were selected for the low- E_{HAD} two-muon analysis based on the following criteria:

- The event vertex was required to be at least 25 cm from any side, 40 cm steel-equivalent from the upstream end and 1.4 m steel-equivalent from the downstream end of the calorimeter.
- At least two muons were required to be found and fitted by the tracking code. At least one of these had to be reconstructed in the toroid spectrometer with a momentum greater than 9 GeV/c.

TABLE I. NuTeV event samples.

	# of events (ν)	# of events ($\bar{\nu}$)
Single muon (all E_{HAD})	1.3×10^6	0.46×10^6
Two muons (all E_{HAD})	4300	1300
Single muon ($E_{HAD} < 3$ GeV)	0.10×10^6	0.06×10^6
Two muons ($E_{HAD} < 3$ GeV)	33	21

- The second muon's momentum could be obtained by either toroid spectrometer or range information; its momentum was required to be at least 5 GeV/c.
- Either the calorimeter drift chamber or scintillator counter signals had to be consistent with passage of two muons over five drift chambers or seven scintillator counters starting at the event vertex.

IV. LOW HADRONIC ENERGY, TWO MUON SOURCES

The analysis strategy consists of comparing data to a model comprised of all known sources of events with two muons and small hadronic energy. Kinematic distributions were generated according to electroweak theory for neutrino trident production, leading order quark-parton model predictions for DIS feed-down, and vector meson dominance (VMD) or partially conserved axial current (PCAC) models extended to four flavors for diffractive charm production. Detector response was modeled using a GEANT-based Monte Carlo (GEANT 3.21), with simulated events processed in an identical fashion as data. The following sections describe the various sources and predictions for their rates.

A. DIS Charm Production

Neutrino DIS produces two major sources of two-muon events. Charged-current charm production can result in a second muon from the decay of the charmed meson (Fig. 3(a)). Also, during charged-current interactions, a π/K in the hadronic shower can decay to a muon and a neutrino before interacting (Fig. 3(b)).

Two-muon events from DIS charm were modeled via leading order predictions using d and s parton distribution functions measured in this and previous experiments [9–13] assuming an effective charm quark mass $m_c = 1.32$ GeV/c². Charm quark fragmentation was treated using

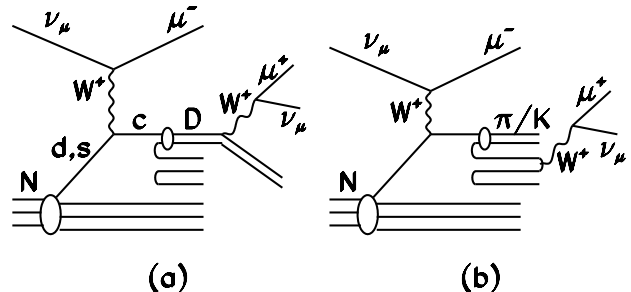


FIG. 3. The Feynman diagrams for DIS production of two-muon events: (a) DIS charged-current production of charm with a semi-muonic decay; (b) DIS charged-current production with a π/K decay in the hadronic shower.

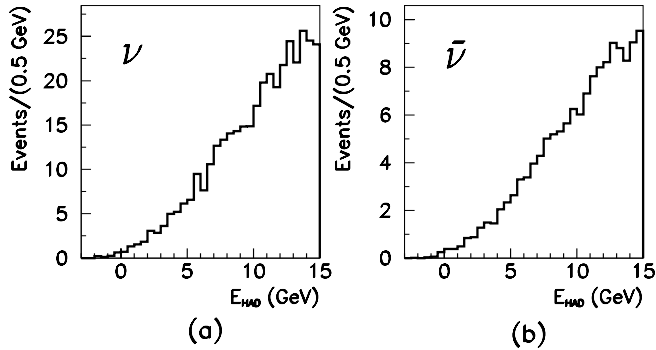


FIG. 4. Distribution of expected hadronic energy (E_{HAD}) for DIS production of two-muon events (Monte Carlo). This analysis is concerned with the contribution near zero.

the Collins-Spiller scheme [14] with fragmentation parameter $\epsilon = 0.93$ and $D^0 : D^+ : \Lambda_C^+$ production ratios measured in Fermilab E531 [15] and corrected for effects of D_S^+ production [16]. Charmed hadron decay was modeled using the best available data as summarized by the Particle Data Group [17], with particular attention given to purely leptonic decays.

Two muon events from π/K decay in the hadron showers of ordinary charged-current (CC) events were modeled using measured parameterizations [18] from a previous experiment (FNAL E744/770) which ran at similar neutrino energies and used the same neutrino target.

The expected hadronic energy (E_{HAD}) spectrum for DIS two-muon Monte Carlo events is shown in Fig. 4. While these sources generally contain significant amounts of hadronic energy, some contribution at low E_{HAD} is seen. Normalizing to the high- E_{HAD} ($E_{HAD} > 5$ GeV) two-muon sample we predict 10.4(4.0) events with $E_{HAD} < 3$ GeV in $\nu(\bar{\nu})$ mode due to the low hadronic energy tail of the DIS process.

B. Neutrino Tridentes

Neutrino trident production is a purely electroweak process in which interference between the charged- and neutral-current diagrams causes a 40% decrease (from $V-A$) in the total cross-section [3,4,19]. Feynman diagrams are shown in Fig. 5. The small ($\sim 10^{-4}$ fb/nucleon) cross-section has limited the observation until recent years [20–22].

For this analysis, the Monte Carlo was generated using the full matrix element with W - Z interference [23,24] including contributions from both coherent nuclear and incoherent nucleon scattering. This procedure incorporated all possible kinematic correlations between the two muons and represents an improvement over previous methods [20,25]. In particular, there is a strong correlation between the energies of the two muons which is very important to the acceptance: when one muon's momentum is high, the other is preferentially very low.

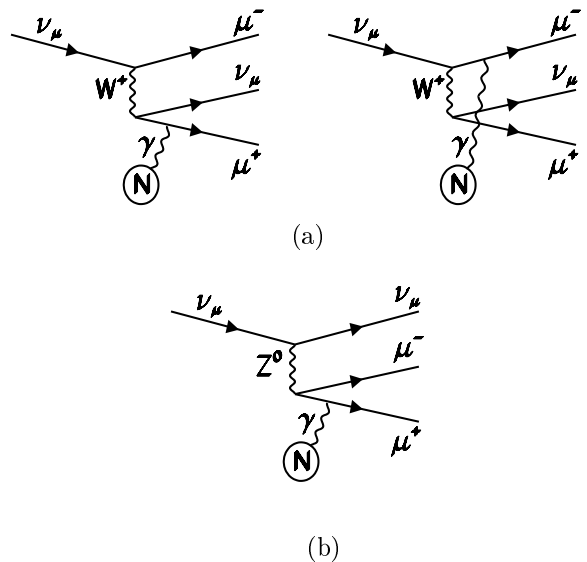


FIG. 5. The Feynman diagrams for neutrino trident production: (a) charged-current production; (b) neutral-current production.

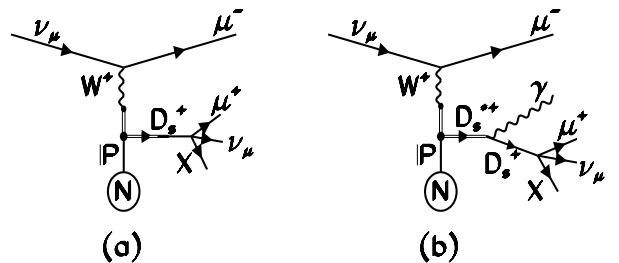


FIG. 6. The Feynman diagrams for (a) D_S^\pm and (b) $D_S^{*\pm}$ production.

The lengthy expression for the cross-section can be found in the references [3,4,19,23,24]. The rate depends on the electroweak mixing angle, which we set to $\sin^2 \theta_W = 0.2222$, and, weakly, on nuclear and nucleon form factors. Standard dipole parameterizations were used for the latter with a vector pole mass $m_V^2 = 0.71$ GeV $^2/c^4$. The nuclear form factor for iron was calculated assuming a Fermi charge density function for iron with nuclear size parameter $c = 3.9$ fm and thickness parameter $b = 0.55$ fm.

NuTeV should observe 4.8(2.2) neutrino trident events in $\nu(\bar{\nu})$ mode from both coherent and incoherent production.

C. $D_S^\pm/D_S^{*\pm}$ Production

Diffractive production of $D_S^\pm(D_S^{*\pm})$ (Fig. 6) has been observed in previous experiments [1,2] and con-

tributes to the low- E_{HAD} two-muon sample whenever the D_S meson decays either to all-lepton final states ($D_S^+ \rightarrow \tau^+ \nu_\tau, \tau^+ \rightarrow \mu^+ \nu_\mu \bar{\nu}_\tau$ or $D_S^+ \rightarrow \mu^+ \nu_\mu$) or to final states with small hadronic energy ($D_S^+ \rightarrow \mu^+ \nu_\mu X_{SOFT}$). The latter case was modeled by assuming that the D_S^+ semi-muonic decay rate was saturated by the channels $D_S^+ \rightarrow \phi \mu^+ \nu_\mu, \eta \mu^+ \nu_\mu, \eta' \mu^+ \nu_\mu$ in the measured proportions summarized by the Particle Data Group [17]. Only contributions from coherent diffractive production were considered. Incoherent production of D_S^+ ($D_S^{*\pm}$) from νN scattering is already included in the inclusive DIS rate.

Vector D_S^* production was modeled assuming a VMD type mechanism with cross-section given by

$$\frac{d^3\sigma(\nu_\mu N \rightarrow \mu D_S^* N)}{dQ^2 d\nu dt} = \frac{Q^2 \nu}{g_\rho^2 E^2} \frac{M_{D_S^*}^2}{(Q^2 + M_{D_S^*}^2)^2} \times \frac{1}{(1-\epsilon)} \frac{e^{-bt}}{b}, \quad (4.1)$$

where Q^2 and ν are the momentum and energy transfer to the D_S^* , t is the square of the momentum transfer to the nucleus, g_ρ is the ρ coupling constant, $M_{D_S^*}$ is the mass of the D_S^* meson, E is the incoming neutrino energy, ϵ is virtual W polarization ($\epsilon = (4E(E-\nu) - Q^2)/(4E(E-\nu) + Q^2 + 2\nu^2)$), and b is the slope of the distribution of momentum transfer squared (t) to the nucleus (nucleon) ($b = 3$ incoherent; $b = 145$ coherent). A check was performed which showed the NuTeV experiment is insensitive to effects of the virtual- W polarization on the D_S^* decay. The overall normalization was left to be determined by the data. To set the scale, the normalization was also obtained in the $SU(4)$ -flavor limit by comparing to the measured cross-section for diffractive ρ^+ production in neutrino scattering.

The number of events expected by NuTeV is normalized to the observed inclusive two-muon data with $E_{HAD} > 5$ GeV

$$N_M = \frac{\int \Phi \times \sigma_M(E_\nu) \times \epsilon(E_\nu) \times BF_M d\Phi}{\int \Phi \times \sigma_{\mu\mu}(E_\nu) \times \epsilon(E_\nu) \times BF_{\mu\mu} d\Phi} \times N_{\mu\mu}, \quad (4.2)$$

where M refers to the meson being produced, $\mu\mu$ refers to DIS two-muon data, Φ is the NuTeV flux, σ is the cross-section, E_ν is the incident neutrino energy, ϵ is the detection efficiency, BF is the (semi-)muonic branching fraction, and $N_{\mu\mu}$ is the number of DIS two-muon events observed in the NuTeV data. This procedure predicts 33.0(13.6) observed D_S^* events for $\nu(\bar{\nu})$ mode in NuTeV.

The contribution of pseudoscalar D_S^+ decay was estimated using PCAC formulas [26,27] adapted for charm:

$$\frac{d^3\sigma(\nu_\mu N \rightarrow \mu D_S N)}{dQ^2 d\nu dt} = \frac{\nu}{E^2} \frac{\epsilon}{(1-\epsilon)} \frac{M_{D_{S1}}^4}{(Q^2 + M_{D_{S1}}^2)^2} \times f_{D_S}^2 \frac{e^{-bt}}{b}, \quad (4.3)$$

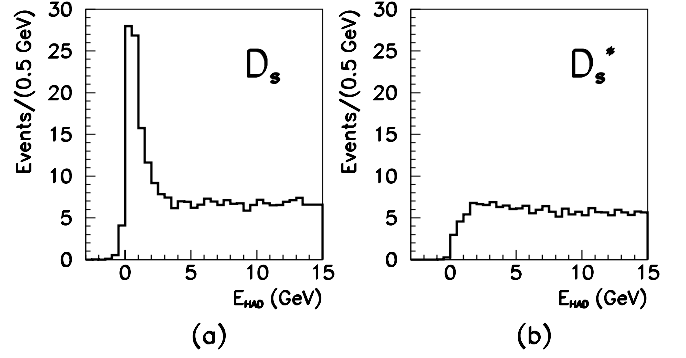


FIG. 7. The E_{HAD} distributions for (a) D_S^\pm and (b) $D_S^{*\pm}$ Monte Carlo.

where $M_{D_{S1}}$ is the mass of the D_{S1} meson and f_{D_S} is the D_S decay constant ($f_{D_S} = 0.31$ GeV). 102.9(48.2) events are predicted for $\nu(\bar{\nu})$ mode in the $SU(4)$ flavor limit.

Figure 7 shows the E_{HAD} distributions predicted by the Monte Carlo. The τ decay mode results in the peak at $E_{HAD} = 0$ for D_S^\pm production while the extra photon from the D_S^\pm decay washes the peak out.

D. Other Sources

Several other contributions to low- E_{HAD} two-muon states contribute at the sub-event level. These include $\mu^+ \mu^-$ decays from neutral-current (NC) diffractively produced J/ψ , $\mu^+ \mu^-$ decays from NC diffractively produced vector mesons, CC diffractively produced π^+ in which the pion decays, π^+ from CC baryon resonance production followed by pion decay, and quasi-elastic CC scattering where pattern recognition errors split the outgoing muon track into two.

1. NC Diffractive Vector Meson Sources

Diffractive production of vector mesons is an important process in photoproduction experiments. A similar process is available in the weak sector with the substitution of a Z^0 for the photon (Fig. 8). Vector mesons which can decay to two muons include ρ^0 , ω , ϕ and J/ψ .

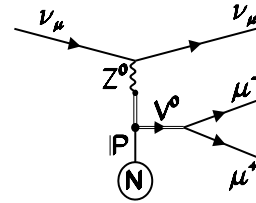


FIG. 8. The Feynman diagram for neutral-current diffractive production of light vector mesons (V^0). Here V^0 can be a ρ^0 , ω , ϕ or J/ψ meson and N represents either a nucleus (coherent) or nucleon (incoherent).

The VMD model is used to predict the expected number of vector mesons. Cross-sections are normalized to the Fermilab E632 measurement of neutrino production of single ρ^\pm [26] with the neutral-current (NC) and charged-current (CC) cross-sections related by Pumplin's procedure [28]. The J/ψ estimate is given in the $SU(4)$ flavor limit for comparison purposes.

Table II lists the number of vector meson events predicted to be observed in the NuTeV data. All sources except J/ψ production are expected to be small, with the suppression largely attributable to the very small $\mu^+\mu^-$ branching fractions for vector mesons. Section VB describes a measurement of the J/ψ signal from diffractive production.

2. Sources from Pion Decay or Mis-reconstruction

Single pions produced in NuTeV have two primary sources: diffractive and resonance production (Fig. 9). The density of the NuTeV detector limits the contribution of both sources to the two-muon sample since the pion must decay prior to interacting. Diffractive production is predicted using the PCAC model normalized to the measured cross-section [26] resulting in 0.08(0.02) estimated events in $\nu(\bar{\nu})$ mode. Resonance production can result in a decay of a final state pion with little visible hadronic energy. This is calculated with a model from Rein and Sehgal [29] and predicts < 0.1 events in either mode.

Quasi-elastic production of Λ_C^\pm events (Fig. 10) has also been considered [30]. The muon from the Λ_C^\pm decay is of very low momentum resulting in extremely low acceptance. We predict < 0.1 events in either mode.

The final source considered was leakage from low- E_{HAD} single muon events due to mis-reconstruction. Contributions from this class of events was greatly reduced by requiring that the scintillator counters or drift chambers were consistent with two muons over a minimum length. The primary remaining source of these events was quasi-elastic scattering where multiple coulomb scattering and drift chamber inefficiencies caused the pattern recognition software to find a spurious second track in the event. This contribution was estimated using straight-through muons which result from

TABLE II. VMD predictions for the expected number of diffractively produced light vector mesons which decay to two muons.

	# of events (coherent) (ν)	# of events (incoherent) (ν)	# of events (coherent) ($\bar{\nu}$)	# of events (incoherent) ($\bar{\nu}$)
ρ^0	0.0074	0.0039	0.0037	0.0019
ω	0.023	0.016	0.011	0.008
ϕ	0.036	0.022	0.018	0.011
J/ψ	4.88	17.1	1.86	7.76

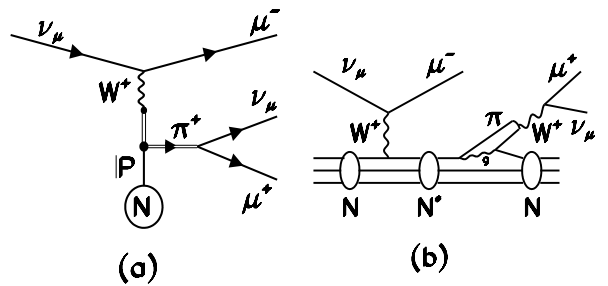


FIG. 9. The Feynman diagrams for single π^\pm production: (a) diffractive and (b) resonance.

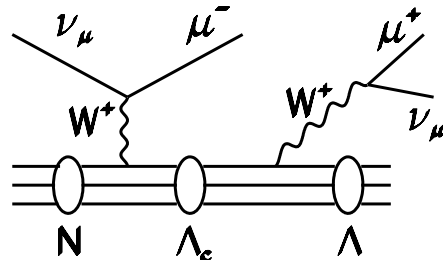


FIG. 10. The Feynman diagram for diffractive Λ_C^\pm production.

charged-current interactions upstream of the detector that enter the calorimeter. A random longitudinal event vertex was chosen, and all event information upstream of this point was discarded, leaving a topology identical to a quasi-elastic event. These straight-through muons were analyzed in the same way as the neutrino data sample and the results normalized to the observed number of single muon quasi-elastic events. The resulting predictions are 0.75(0.25) events in $\nu(\bar{\nu})$ mode.

A summary of the predicted number of events from each source is shown in Table III. The remainder of this paper describes the measurement of the largest sources: DIS, neutrino tridents, $D_S^\pm / D_S^{*\pm}$, and J/ψ .

V. RESULTS

A. Charged-Current Analysis

Our charged-current analysis examines three kinematic variables: the hadronic energy (E_{HAD}) up to 15 GeV, the two-muon invariant mass ($M_{\mu\mu}$), and the absolute value of the smallest difference between the muon azimuthal angles ($\Delta\phi$). Distributions for these quantities as measured in NuTeV data are shown in Figs. 11, 12, 13, and 14. Since the analysis is primarily concerned

TABLE III. Predictions for the number of events expected to be observed by NuTeV in the low- E_{HAD} ($E_{HAD} < 3$ GeV) two-muon sample.

	# of events (ν)	# of events ($\bar{\nu}$)	
DIS	10.4	4.0	Ref. [9]
Neutrino Tridents	4.8	2.2	Ref. [3,4]
D_S^\pm	102.9	48.2	Ref. [1,2]
$D_S^{*\pm}$	33.0	13.6	Ref. [1,2]
Light vector mesons (ρ^0, ω, ϕ)	< 0.12	< 0.08	Ref. [26,28]
J/ψ (coherent)	4.88	1.86	Ref. [26,28]
J/ψ (incoherent)	17.1	7.76	Ref. [26,28]
Single π^\pm	< 0.1	< 0.1	Ref. [26,29]
Λ_C^\pm	< 0.1	< 0.1	Ref. [30]
Mis-identified single muon events	0.75	0.25	
Sum	174.4	78.2	

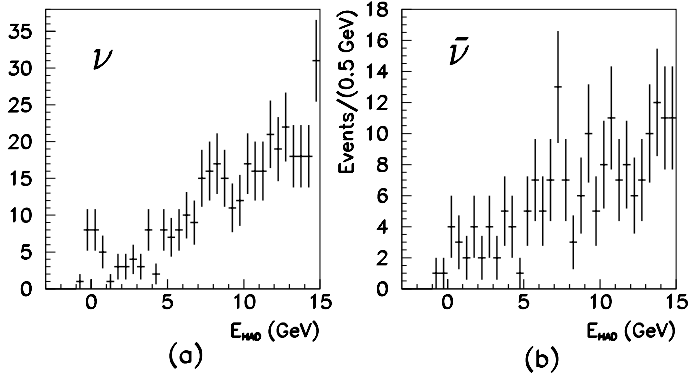


FIG. 11. The hadronic energy distribution for the two-muon data. The first twelve bins contribute to figures 13 and 14.

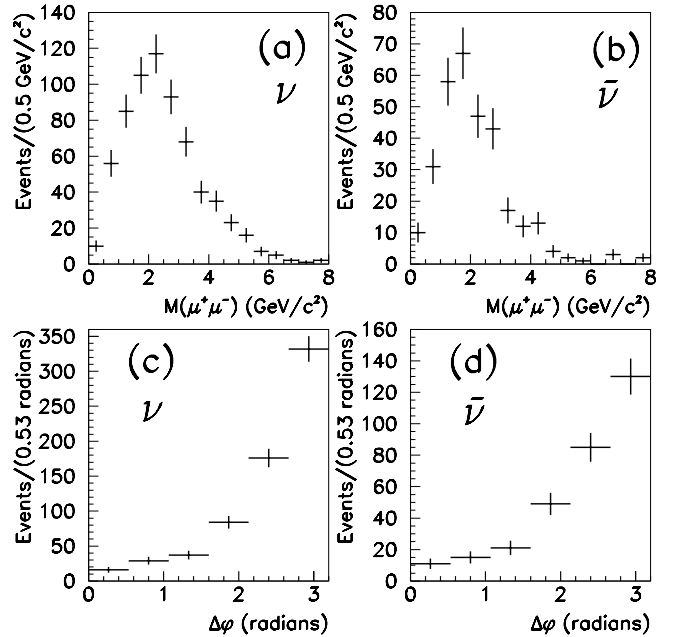


FIG. 12. Distributions for the two-muon NuTeV events with $E_{HAD} < 15$ GeV. The plots are the two-muon invariant mass ($M_{\mu\mu}$) for ν (a) and $\bar{\nu}$ (b) modes and $\Delta\phi$ in ν (c) and $\bar{\nu}$ (d) modes.

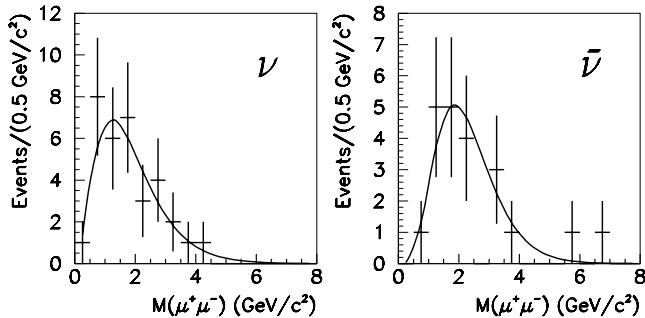


FIG. 13. The two-muon invariant mass ($M_{\mu\mu}$) for the low- E_{HAD} ($E_{HAD} < 3$ GeV) two-muon data. The curve shows a fit to the distribution $x^\alpha e^{-(\beta+\gamma x)}$.

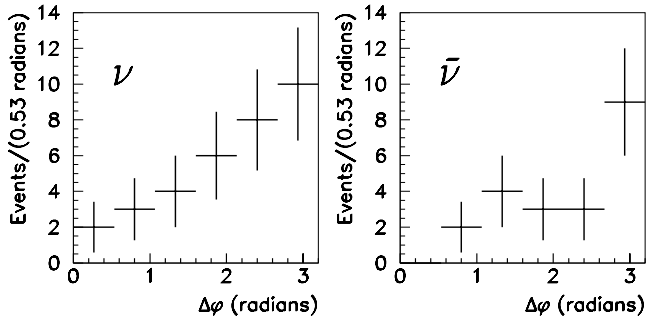


FIG. 14. The $\Delta\phi$ distributions for the low- E_{HAD} ($E_{HAD} < 3$ GeV) two-muon data. $\Delta\phi$ is defined in the text.

with events that peak at low E_{HAD} , the $M_{\mu\mu}$ (Fig. 13) and $\Delta\phi$ (Fig. 14) distributions are plotted with the additional restriction $E_{HAD} \leq 3$ GeV to emphasize the diffractive region. However, all events with $E_{HAD} \leq 15$ GeV are used in the subsequent fitting. Thirty-three neutrino and 21 anti-neutrino two-muon events were observed with $E_{HAD} < 3$ GeV. These numbers are significantly below the sum of the predicted number of events in Table III, indicating the naive $SU(4)$ flavor predictions for heavy quark final states are too large. On the other hand, there is a large excess over the predictions from DIS feed-down and neutrino trident production.

A fit was performed allowing up to four sources of low- E_{HAD} two-muon events: DIS, neutrino tridents, diffractive D_S^\pm , and diffractive $D_S^{*\pm}$. These sources were simulated via Monte Carlo and normalized to the NuTeV inclusive two-muon samples. Figure 15 shows distributions of E_{HAD} , $M_{\mu\mu}$, and $\Delta\phi$ for the four major sources. Deep-inelastic scattering contributions peak at high $M_{\mu\mu}$,

high E_{HAD} , and at $\Delta\phi = 0$ and π , the latter feature reflecting the essentially two-body final state of DIS charm production. The neutrino trident signal peaks at low E_{HAD} , low $M_{\mu\mu}$ and is more uniform in $\Delta\phi$. The D_S and D_S^* distributions are intermediate between DIS and neutrino tridents, with D_S distinguishable from D_S^* in the E_{HAD} distribution due to the decay photon contribution to E_{HAD} for D_S^* . Diffractive D_S and neutrino trident distributions are very similar, hence their measurements are highly correlated.

Data and Monte Carlo were binned three-dimensionally in $(E_{HAD}, M_{\mu\mu}, \Delta\phi)$ space: 18 bins in E_{HAD} (-3 - 15 GeV), 6 in $M_{\mu\mu}$ (0 - 6 GeV); and 6 in $|\Delta\phi|$ (0 - π radians). The Monte Carlo is fit to the data using a maximum-likelihood technique. The Monte Carlo sets are summed together using a single normalization factor for each source which was defined to be 1.0 for the level presented in the preceding section. Neutrino and anti-neutrino modes were fit simultaneously.

The results of the fit are shown in Table IV. Figure 16 compares these results to the data and shows we are able to describe the data with the four largest sources. The DIS contribution is consistent with that expected from the higher E_{HAD} two-muon analysis [9]. The neutrino trident contribution is consistent with the Standard Model prediction, but can not distinguish between V-A and the Standard Model. This is in contrast to previous analyses which ruled out V-A but did not consider diffractive sources.

TABLE IV. Parameters from the three parameter fit to the low- E_{HAD} two-muon data.

Parameter	Result
DIS	+0.09 -0.08
Neutrino Tridents	+1.73 -0.72
Diffractive Charm ($D_S^\pm + D_S^{*\pm}$)	+0.06 -0.06

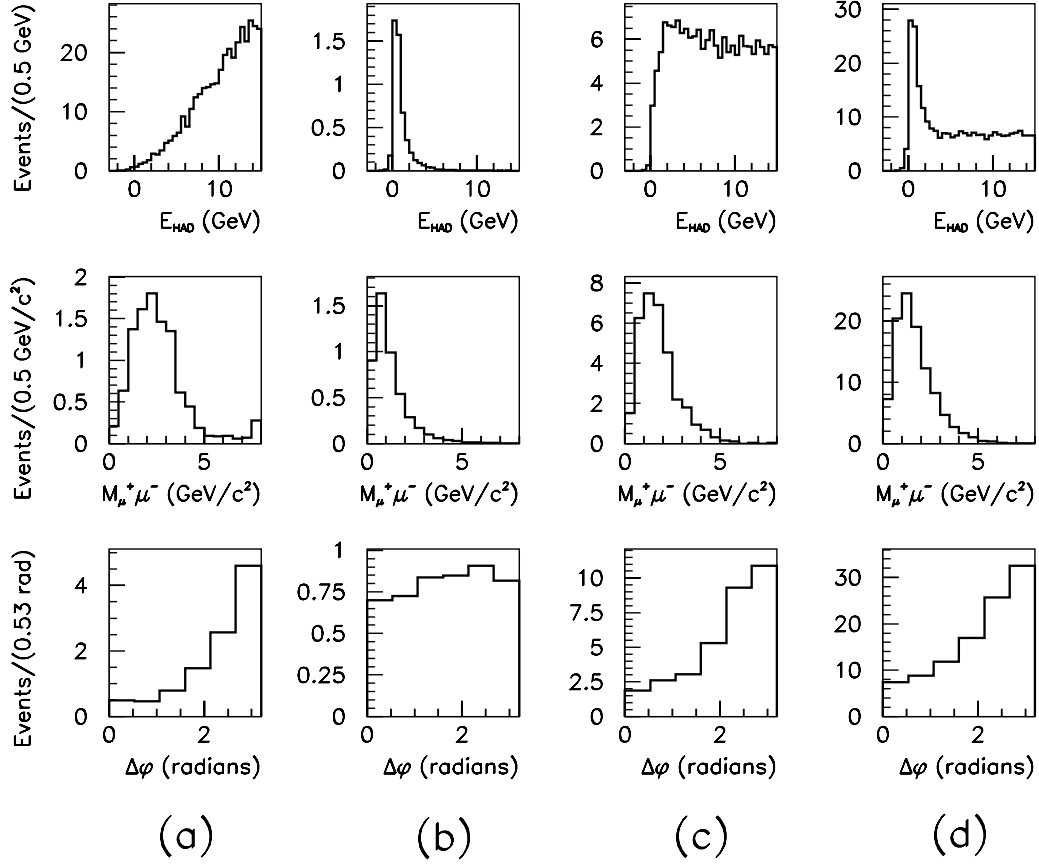


FIG. 15. Monte Carlo distributions of visible hadronic energy, two muon invariant mass and $\Delta\phi$ for the four the four largest sources of low- E_{HAD} two-muon events: (a) DIS charm; (b) neutrino tridents; (c) diffractive D_S^\pm ; (d) diffractive $D_S^{*\pm}$. The invariant mass and $\Delta\phi$ distributions are for $E_{HAD} < 3$ GeV.

TABLE V. Measured event contributions to the low- E_{HAD} two-muon event sample.

	# of events (ν)	# of events (ν)
J/ψ (90% CL)	<7.5	<5.0
DIS	+0.9 -0.9	+0.4 -0.4
Neutrino Tridents	+8.3 -3.5	+3.8 -1.6
$(D_S^\pm + D_S^{*\pm})$	+8.1 -8.2	+3.7 -3.7
Mis-identified single muon events	0.75 ± 0.43	0.25 ± 0.25
All other sources (estimate)	<0.1	<0.1

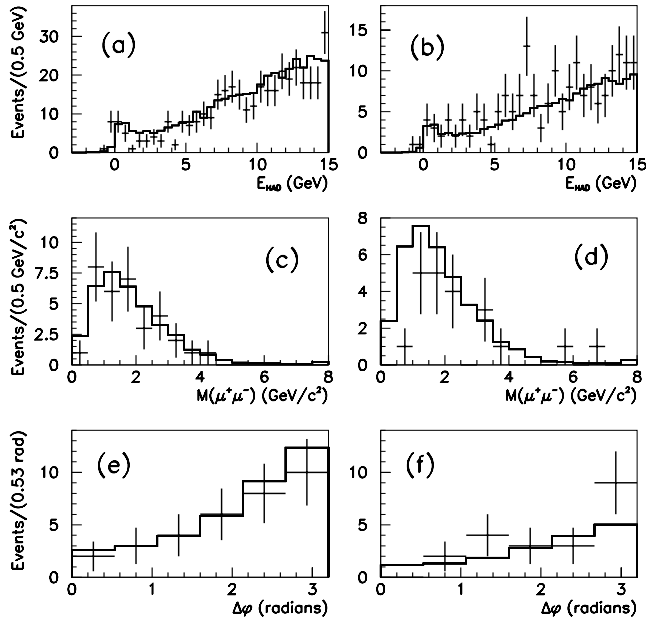


FIG. 16. Comparison of the final result (MC) to the low- E_{HAD} two-muon data for (a,b) E_{HAD} , (c,d) $M_{\mu^+\mu^-}$, (e,f) $\Delta\phi$. The left side is ν mode; the right side is $\bar{\nu}$ mode. The $M_{\mu^+\mu^-}$ and $\Delta\phi$ distributions are for $E_{HAD} < 3$ GeV. The points represent the data while the histogram shows the Monte Carlo.

The consideration of all sources of low- E_{HAD} two-muon events allows us to measure diffractive charm production. The D_S^\pm and $D_S^{*\pm}$ sources have been combined in proportion to the theoretical predictions and a single fit parameter used. This yields cross-sections of

$$\sigma(\nu_\mu Fe \rightarrow \mu^-(D_S + D_S^*)Fe) = (3.3 \pm 1.1) \text{ fb/nucleon},$$

evaluated at $E_\nu = 130$ GeV using the modified VMD and PCAC predictions to extrapolate in energy under the assumptions $\sigma(\nu_\mu Fe \rightarrow \mu^- D_S^{*+} Fe) = \sigma(\bar{\nu}_\mu Fe \rightarrow \mu^+ D_S^{*-} Fe)$ and $\sigma(\nu_\mu Fe \rightarrow \mu^- D_S^+ Fe) = \sigma(\bar{\nu}_\mu Fe \rightarrow \mu^+ D_S^- Fe)$. A second fit performed with the neutrino trident parameter fixed to the Standard Model prediction yielded the consistent results $\sigma(\nu_\mu Fe \rightarrow \mu^-(D_S + D_S^*)Fe) = (3.0 \pm 0.8) \text{ fb/nucleon}$ at $E_\nu = 130$ GeV. The quoted errors are completely dominated by statistics. This result assumes an isotropic D_S^* decay. Studies showed effects of a possible D_S^* polarization to be small. The largest change, corresponding to nearly complete longitudinal polarization, lowered $\sigma(D_S + D_S^*)$ by 0.4 fb/nucleon.

Previously, the Big Bubble Chamber Neutrino Collaboration combined various data samples to measure the diffractive rate of charmed strange mesons ($D_S^\pm + D_S^{*\pm}$) per charged-current νI (I is an isoscalar target) interaction [1]. They measured a rate of $(2.8 \pm 1.1) \times 10^{-3}$. The observation of $D_S^{*\pm}$ production by CHORUS [2] is in agreement with this rate. Using the results of our second fit, we find a rate of $(3.2 \pm 0.6) \times 10^{-3}$, which is

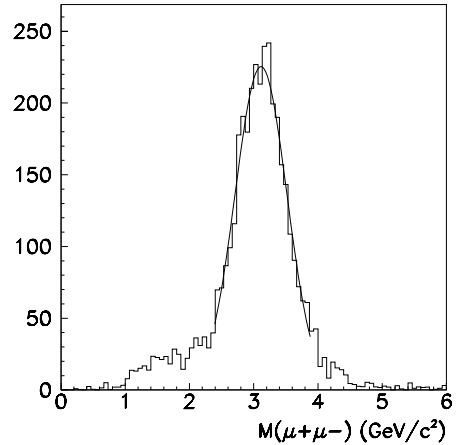


FIG. 17. The two muon invariant mass ($M_{\mu\mu}$) for the J/ψ Monte Carlo. The curve shows a Gaussian fit.

consistent with previous results.

Table V lists the number of events contribution of each source in the low- E_{HAD} two muon data sample as determined by this analysis.

B. Neutral-Current Analysis

Neutral-current J/ψ production produces a clear signature in the two muon invariant mass, particularly if $E_{HAD} \leq 3$ GeV is imposed to select diffractively produced events. There is no evidence for a J/ψ signal in Fig. 13; however, the relatively poor resolution of the NuTeV detector may be obscuring a contribution from this source. To assess this possibility, a diffractive J/ψ sample was simulated via Monte Carlo to obtain the $M_{\mu\mu}$ distribution shown in Fig. 17. A Gaussian fit to this distribution yields a resolution $\sigma_0 = 0.40 \text{ GeV}/c^2$.

A maximum likelihood fit was then performed to determine the amount of J/ψ present in the data. The fit function was taken to be

$$N(M_{\mu\mu}) = M_{\mu\mu}^\alpha e^{(\beta+\gamma M_{\mu\mu})} + A \times e^{-\frac{1}{2}(\frac{M_{\mu\mu}-M_0}{\sigma_0})^2}, \quad (5.1)$$

where $M_{\mu\mu}$ is the two muon invariant mass. M_0 and σ_0 are the mass and width of the J/ψ as measured by the Monte Carlo. The first term represents a smooth parameterization of the background description where α and γ determine the shape and β the normalization. The second term is a Gaussian description of the J/ψ contribution with mean mass M_0 and width σ_0 set to the Monte Carlo prediction. The parameter A measures the amount of J/ψ in the data.

The results of the fit are shown in Table VI. A 90% confidence level (CL) on the J/ψ contribution is set by fixing the J/ψ amplitude to various increasing levels and fitting for the background. The likelihood function ($\mathcal{L}(A)$) was plotted as a function of A and the 90% CL limit set by $\int_{A_0}^{A_{CL}} \mathcal{L}(A) dA / \int_{A_0}^{\infty} \mathcal{L}(A) dA = 0.90$. The

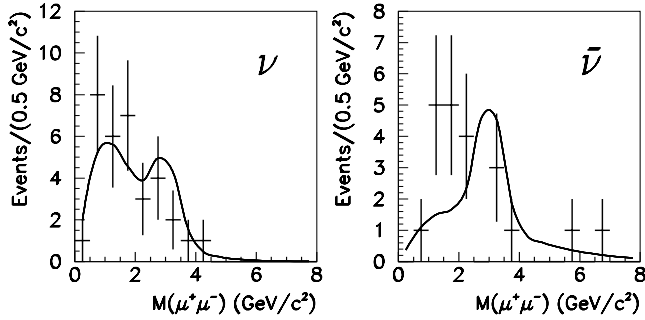


FIG. 18. 90% confidence level limit on diffractive J/ψ production. The curve shows the fit to the background with the 90% CL contribution from J/ψ .

resulting number of events is found by integrating the Gaussian with amplitude A_{CL} and converting to a cross-section by normalizing to the DIS two-muon sample. The 90% confidence level limits on the diffractive J/ψ cross-section are

$$\sigma(\nu_\mu Fe \rightarrow \nu_\mu J/\psi Fe) \leq 0.21 \text{ fb/nucleon at 90\% CL,}$$

$$\sigma(\bar{\nu}_\mu Fe \rightarrow \bar{\nu}_\mu J/\psi Fe) \leq 0.36 \text{ fb/nucleon at 90\% CL,}$$

at a mean production energy of $E_\nu = 175$ GeV for $E_{HAD} \leq 3$ GeV. Figure 18 shows the results of this limit including the J/ψ contribution.

Using the VMD model, we can extrapolate the J/ψ cross-section to lower E_ν to compare to the CDHS measurement of (0.042 ± 0.015) fb/nucleon. Figure 19 shows a 90% CL limit for the J/ψ cross-section normalized to the NuTeV measurement and compares to the CDHS result. The energy dependence of this limit is dependent upon the model inputs. We show the limit for a momentum transfer squared (t) distribution of e^{-145t} [26] and coherent production only. The interpretation of the

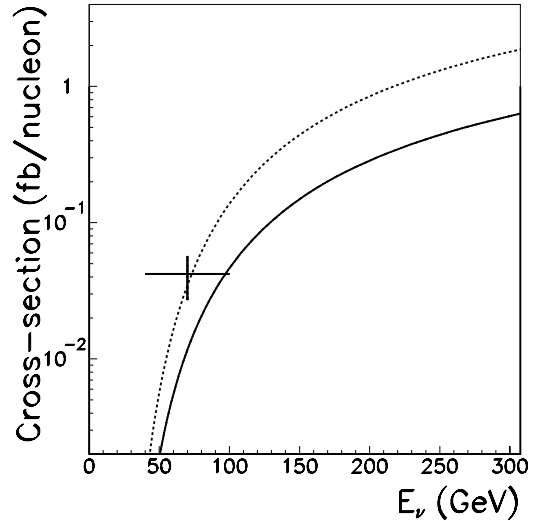


FIG. 19. Energy dependence of the 90% confidence level limit on diffractive J/ψ production normalized to the NuTeV measurement. The solid line is the limit set with $E_{HAD} < 3$ GeV and the dashed line with $E_{HAD} < 10$ GeV. The data point shows the CDHS measurement.

CDHS measurement as diffractive production is contradicted by our limit; however, the CDHS E_{HAD} cut of 10 GeV compared to a mean neutrino energy of 70 GeV could have accepted DIS production of J/ψ .

The analysis was repeated with a higher E_{HAD} cut ($E_{HAD} < 10$ GeV) which matches the CDHS selection. The results are also included in Table VI. The limit as a function of E_ν is shown as the dashed curve in Fig. 19. While this limit is near the CDHS measurement, the diffractive J/ψ Monte Carlo shows the lower E_{HAD} (< 3 GeV) is appropriate for coherent diffractive production. One possible explanation is that the higher cut allows a contribution from DIS J/ψ production.

TABLE VI. Limits on diffractive J/ψ production observed by NuTeV in the low- E_{HAD} two-muon sample.

	ν mode	$\bar{\nu}$ mode
$E_{HAD} < 3$ GeV		
# of events (fit)	3.3 ± 5.0	-1.7 ± 4.0
# of events (90% CL)	7.5	5.0
Average E_ν (J/ψ) (GeV)	185.0	168.0
Cross-Section (90% CL) ($E_\nu = 175$ GeV) (fb/nucleon)	0.19	0.32
Cross-Section (90% CL) ($E_\nu = 70$ GeV) (fb/nucleon)	0.011	0.017
$E_{HAD} < 10$ GeV		
# of events (fit)	7.8 ± 14.3	-2.4 ± 10.5
# of events (90% CL)	24.8	11.5
Cross-Section (90% CL) ($E_\nu = 175$ GeV) (fb/nucleon)	0.63	0.73
Cross-Section (90% CL) ($E_\nu = 70$ GeV) (fb/nucleon)	0.034	0.040
CDHS result ($E_{HAD} < 10$ GeV)		
Cross-Section (Fit) ($E_\nu = 70$ GeV) (fb/nucleon)	(0.042 ± 0.015)	

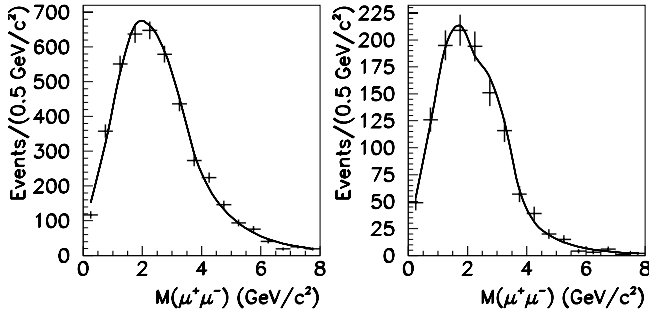


FIG. 20. The two muon invariant mass distribution for high- E_{HAD} ($E_{HAD} > 10$ GeV). The curve shows the fit to the background with the 90% CL contribution from J/ψ .

For completeness, the E_{HAD} cut was changed to $E_{HAD} > 10$ GeV to allow a search for inclusive DIS J/ψ production. Figure 20 shows the resulting $M_{\mu\mu}$ distribution. A fit was performed with the background modelled by an asymmetric Gaussian function and the data binned in 0.5 GeV/ c^2 intervals. No statistically significant J/ψ signal was found, and 90% confidence level limits for the (DIS J/ψ)/(DIS CC charm) rates were found to be

$$\frac{N(\nu_\mu N \rightarrow \nu_\mu J/\psi X)}{N(\nu_\mu N \rightarrow \mu^- cX)} \leq 0.024 \text{ at 90\% CL,}$$

$$\frac{N(\bar{\nu}_\mu N \rightarrow \bar{\nu}_\mu J/\psi X)}{N(\bar{\nu}_\mu N \rightarrow \mu^+ cX)} \leq 0.069 \text{ at 90\% CL,}$$

when averaged over the NuTeV beam spectra. Assuming a similar energy dependence to DIS CC charm production, this corresponds to cross-section limits evaluated at $E_\nu = 125$ GeV,

$$\sigma(\nu_\mu N \rightarrow \nu_\mu J/\psi X) \leq 2.2 \text{ fb/nucleon at 90\% CL,}$$

$$\sigma(\bar{\nu}_\mu N \rightarrow \bar{\nu}_\mu J/\psi X) \leq 3.4 \text{ fb/nucleon at 90\% CL,}$$

at an average DIS CC charm production energy of $E_\nu = 125$ GeV. Figure 20 shows the 90% CL curve for the inclusive ($E_{HAD} > 10$ GeV) DIS two-muon sample.

VI. CONCLUSIONS

We have performed an inclusive analysis of the low- E_{HAD} two-muon data sample available from NuTeV. All known Standard Model processes have been considered, and four significant sources were found to contribute: DIS, neutrino trident, diffractive D_S^\pm , and diffractive $D_S^{*\pm}$. We have measured diffractive D_S^\pm and $D_S^{*\pm}$ cross-sections to be 1.4 ± 0.4 fb/nucleon and 1.6 ± 0.5 fb/nucleon, respectively, for $\nu_\mu Fe$ scattering at $E_\nu = 130$ GeV, in agreement with previous results assuming a

VMD energy dependence of the cross-section. We observe a statistically weak neutrino trident signal consistent with Standard Model predictions. Finally, we see no evidence for either diffractive or DIS production of J/ψ in NC ν_μ and $\bar{\nu}_\mu$ scattering on iron.

ACKNOWLEDGMENTS

We would like to thank the staffs of the Fermilab Particle Physics and Beams Divisions for their contributions to the construction and operation of the NuTeV beamlines. We would also like to thank the staffs of our home institutions for their help throughout the running and analysis of NuTeV. This work has been sponsored by the U.S. Department of Energy and the National Science Foundation.

-
- [1] A. E. Asratyan *et al.*, Z. Phys. **C 58**, 55 (1993).
 - [2] P. Annis *et al.*, Phys. Lett. **B 435** 458 (1998).
 - [3] R. Belusevic and J. Smith, Phys. Rev. **D 37**, 2419 (1987).
 - [4] C. H. Llewellyn Smith, Phys. Rept. **3** 261 (1972).
 - [5] H. Abramowicz *et al.*, Phys. Lett. **109B**, 115 (1982).
 - [6] W. S. Sakumoto *et al.*, Nucl. Instrum. Methods. **A 294**, 179 (1991); B. J. King *et al.*, Nucl. Instrum. Methods. **A 302** 254 (1991).
 - [7] R. H. Bernstein *et al.*, NuTeV Collaboration, "Technical Memorandum: Sign Selected Quadrupole Train," FERMILAB-TM-1884 (1994); J. Yu *et al.*, NuTeV Collaboration, "Technical Memorandum: NuTeV SSQT performance," FERMILAB-TM-2040 (1998).
 - [8] D. Harris, J. Yu *et al.*, HEP-EX/9908056, (submitted to Nucl. Instrum. Methods A).
 - [9] T. Adams *et al.*, in *Proceedings of the 33rd Rencontres de Moriond, QCD and Hadronic Interactions*, (to be published).
 - [10] P. Vilain *et al.*, CERN-EP/98-128 (1998).
 - [11] A. O. Bazarko *et al.*, Z. Phys. **C 65** 189 (1995).
 - [12] S. A. Rabinowitz *et al.*, Phys. Rev. Lett. **70**, 134 (1993).
 - [13] H. Abramowicz *et al.*, Z. Phys. **C 15**, 19 (1982).
 - [14] P. Collins and T. Spiller, J. Phys. **G 11**, 1289 (1985).
 - [15] N. Ushida *et al.*, Phys. Lett. **B206**, 375 (1988).
 - [16] T. Bolton, HEP-EX/970814 (1997).
 - [17] Particle Data Group, Eur. Phys. J. **C 3** (1998).
 - [18] P. H. Sandler, Ph.D. thesis, University of Wisconsin-Madison, (1992).
 - [19] R. W. Brown *et al.*, Phys. Rev. **D6**, 3273 (1972).
 - [20] S. R. Mishra *et al.*, Phys. Rev. Lett. **66**, 3117 (1991).
 - [21] G. Geiregat *et al.*, Phys. Lett. **B 245**, 271 (1990).
 - [22] F. Bergsma *et al.*, Phys. Lett. **B 122**, 185 (1983).
 - [23] K. Fujikawa, Ann. Phys. **68**, 102 (1971); K. Fujikawa, Ann. Phys. **75**, 491 (1973).
 - [24] K. Fujikawa, Phys. Rev. **D 8**, 1623 (1973).
 - [25] T. Adams *et al.*, in *Proceedings of the 29th International*

Conference on High Energy Physics, Vancouver, Canada, 1998, edited by Alan Astbury, David Axen, and Jacob Robinson, p. 631.

- [26] S. Willocq *et al.*, Phys. Rev. **D47**, 2661 (1993).
- [27] B. Z. Kopeliovich and P. Marage, Int. Jour. Mod. Phys. **A 8**, 1513 (1993).
- [28] J. Pumplin, Phys. Rev. Lett. **64**, 2751 (1990).
- [29] D. Rein and L. M. Sehgal, Ann. Phys. **133**, 79 (1981).
- [30] R. E. Shrock and B. W. Lee, Phys. Rev. **D 13**, 2539 (1976); Erratum-ibid **D 14**, 313 (1976).